Dynamical evolution of Rayleigh-Taylor and Richtmyer-Meshkov mixing fronts

Baolian Cheng
Applied Physics Division, Los Alamos National Laboratory, Los Alamos, New Mexico 87545

J. Glimm
Department of Applied Mathematics and Statistics, University at Stony Brook, Stony Brook, New York 11794-3600 and Center for Data Intensive Computing, Brookhaven National Laboratory, Upton, New York 11793-5000

D. H. Sharp
Applied Physics Division, Theoretical Division, Los Alamos National Laboratory, Los Alamos, New Mexico 87545

(Received 17 May 2001; revised manuscript received 11 June 2002; published 25 September 2002)

Dynamic behavior of mixing fronts plays a crucial role in multifluid turbulent mixing. In this paper, we derive an analytic solution for the dynamic evolution of mixing fronts driven by constant acceleration Rayleigh-Taylor (RT) and impulsive acceleration Richtmyer-Meshkov instabilities, from a simple physics model expressed as a pair of ordinary differential equations. An approximate closed form asymptotic evaluation of the RT solution is obtained, through terms of order $O(1)$, as $t\to\infty$. This three term expansion, including lower order terms, is used to interpret experimental and simulation data. Our solutions improve on previous analyses in their agreement with experimental data, in that we can fit both the slope and the intercept of the Z_b vs Agt^2 experimental plots by adjusting parameters in our model. Since the experimental data are close to self-similar, the improvement due to the lower order contributions in the asymptotic expansion is modest. We also apply this analysis to simulation data, for which preasymptotic data exist. We reexamine previous simulation data and determine an improved growth rate $\alpha_b=0.0625$. The present paper provides concepts and tools to explore the preasymptotic aspects of these data.

DOI: 10.1103/PhysRevE.66.036312 PACS number(s): 47.20.Ma, 47.52.+j

I. INTRODUCTION

Chaotic mixing is a common and important phenomenon in basic science and in engineering applications. Small disturbances in a multifluid system produce buoyancy and shear driven instabilities at an interface between distinct fluids [1]. These instabilities grow and develop into turbulent mixing zones consisting of bubbles of light fluid and spikes of heavy fluid, each penetrating into the opposite fluid. The evolution and structure of these mixing zones have been studied for several decades, see, for example, Refs. [2–5]. The location of the two edges of the mixing zone plays a distinguished role, as the simplest and primary descriptor of the mixing process. The study of mixing processes is not only of theoretical interest. It also plays an important role in the study of inertial confinement fusion and late time supernova evolution.

The main contribution of the present work is to provide a detailed solution, expressed in closed form up to quadratures, for the entire dynamical evolution of the two mixing zone edges for the Rayleigh-Taylor (RT) instability. The solution is obtained through integration of an explicit differential equation for the mixing zone edges. The large time asymptotics of this solution are derived in closed form. The lower than leading order asymptotics display dependence on initial conditions for RT mixing, and their closed form expression contains approximations. This fact allows an improvement in the fit of theory to experimental data. Reinterpretation of RT simulation mixing rate data is also discussed.

II. MOTION OF THE BOUNDARY

The nonlinear evolution of the edge of a mixing zone resulting from (incompressible) RT or Richtmyer-Meshkov (RM) unstable flows, can be described by the phenomenological equation

$$(\rho_i+k_i\rho_{i'})\frac{dV_i}{dt}=(\rho_i-\rho_{i'})g(t)-(-1)^i\frac{C_i\rho_{i'}V_i^2}{|Z_i|},\quad i=1,2. \tag{1}$$

Here $i=1=b$ (bubble) and $i=2=s$ (spike) denote the light and heavy fluids, respectively. The index of the phase opposite to i is $i'=3-i$. Also $V_i\equiv dZ_i/dt$ is the velocity of the edge i of the mixing zone. We assume that $(-1)^iV_i(t)>0$ for all t. Also $g(t)$ is the gravitational acceleration, k_i is an added mass coefficient due to the existence of fluid i', ρ_i is the mass density of fluid i, and C_i is a phenomenological drag coefficient for the edge of fluid i.

Equation (1) has been divided by the volume for the purpose of normalization. Since the total drag force on a bubble or spike is proportional to its frontal surface area, upon dividing by this volume one is left with a longitudinal length scale, given in our model by $|Z_i|$. The form of the drag force reflects the assumption that the fluid infinitely far upstream of the bubble or spike is stagnant.

The added mass parameter k_i allows consideration of distinct flow regimes. We consider cylindrical bubbles and spikes (i.e., three-dimensional bubbles and spikes connected continuously to their ambient phase). Youngs [7] allows a renormalization coefficient in front of the buoyancy term,

which we set to unity here. This choice is consistent with our overall objective of minimizing the number of experimentally determined parameters in our model, and thus to maximize the fraction of the limited experimental data which is actually predicted (rather than fit) by the model. Determination of the drag coefficient C_i and validation of Eq. (1) through comparison with experiment was presented in Ref. [6].

Spherical front bubbles and spikes, representing a post breakup configuration of the bubble and spike tips, disconnected from the ambient portion of their own phase, are also modeled by Eq. (1), but with a modified choice of the added mass k_i. It is common to replace the length $|Z_i|$ in Eq. (1) by a length L having its own dynamical evolution law. Finely dispersed flows would then have a smaller value of L, reflecting their smaller length scale.

A basic assumption of our analysis is that RT and RM mixing can be described by a single ordinary differential equation (ODE) with common drag and added mass coefficients. In a previous study [6] this assumption was shown to lead to results in good agreement with the existing experimental data on RT and RM instability. Equation (1) states that the acceleration of an edge arises from the net effect of buoyancy and drag forces, an idea that was proposed for RT instability by Youngs [7]. Force laws similar in form were used by Alon *et al.* [8,9] and Dimonte *et al.* [10–12] to analyze the trajectories of the spike and bubble fronts in RT and RM instabilities. In previous work a self-similar solution is assumed and the bubble growth rate is determined by substitution of the assumed solution into the equation. Here we derive an analytic solution for the entire evolution of the RT mixing fronts in terms of the physical parameters (A, C_i, k_i) and the initial conditions. Therefore, this work provides a physical understanding for the self-similarity assumed in the other models. The dynamical transition of the system from an early (but still chaotically mixing) behavior to the late self-similarity regime is clearly displayed, and the dependence of the lower than leading order RT solution asymptotics on initial conditions is obtained. We also present an analysis of experimental data that provides a physical interpretation of the meaning of the intercepts of the h vs Agt^2 line with the coordinate axes. Finally, an analysis of simulation data offers a possible explanation for the deviation of the h vs Agt^2 curve from a straight line. A significant difference between our model and related models appearing in the literature is in the treatment of the drag term in Eq. (1). In our model we have consistently [6] used the ambient fluid density $\rho_{k'}$, as discussed by Landau [13], instead of the displacing fluid density ρ_k used in work of others [8–12] (a correction to some of the cited work has recently appeared [14]). Our expression leads to finite values of C_i in the limit of $A=1$ in contrast to the otherwise zero (infinite) drag coefficient describing a vacuum bubble (spike) rising in a fluid (vacuum). Also our expression gives A-dependent drag coefficients if the RT bubble mixing rate α_b is independent of Atwood number A. These results are consistent with both experiments and numerical simulations [7].

For cylindrical bubbles and spikes, we set $k_i \sim 1$, and Eq. (1) becomes

$$\frac{dV_i}{dt} = (-1)^i Ag(t) - (-1)^i C_i \frac{1-(-1)^i A}{2} \frac{V_i^2}{|Z_i|}, \quad i=1,2, \tag{2}$$

where the drag coefficient C_i is given by [6]

$$C_i = \frac{1/\alpha_i - [1-(-1)^i A] - k_i[1-(-1)^i A]}{2[1-(-1)^i A]}, \tag{3}$$

in which α_i is the growth rate of fluid i in the self-similar regime of RT mixing and $A \equiv (\rho_2-\rho_1)/(\rho_2+\rho_1)$ is the Atwood number.

III. RT MIXING FRONTS

Assume steady acceleration, so that $g(t)=g$ is independent of time t in Eq. (2). In order to solve the ODE (2), we work with scaled variables. Let $V_i' \equiv V_i/\sqrt{Ag|Z_i|}$ represent the scaled velocity of the RT mixing fronts and $dt' \equiv dt\sqrt{Ag/|Z_i|}$ the scaled differential time. Then the front acceleration $dV_i/dt = \sqrt{Ag|Z_i|}\,dV_i'/dt + AgV_i'^2/2 = Agd V_i'/dt' + AgV_i'^2/2$. With these scaled variables, Eq. (2) becomes

$$\frac{dV_i'}{dt'} = (-1)^i - \frac{(-1)^i}{2}\{1 + C_i[1-(-1)^i A]\}V_i'^2. \tag{4}$$

Noting that $|V_i'| = (-1)^i V_i'$, Eq. (4) can be rewritten as

$$\frac{d|V_i'|}{dt'} = 1 - \tfrac{1}{2}\{1 + C_i[1-(-1)^i A]\}|V_i'|^2. \tag{5}$$

As shown in Ref. [6], the drag coefficient C_i is a function of A alone. For fixed A, C_i is a constant. Let $a_i^2 \equiv \frac{1}{2}\{1 + C_i[1-(-1)^i A]\}$. We integrate Eq. (4) to obtain

$$t' - t_0' = \frac{1}{2a_i} \ln \frac{(1+a_i|V_i'|)f_{i0}}{1-a_i|V_i'|}, \tag{6}$$

where $f_{i0} \equiv (1-a_i|V_{i0}'|)/(1+a_i|V_{i0}'|)$, $|V_{i0}'| \equiv |V_i'(t_0')|$, and $t_0' \equiv t'(t=t_0)$ are determined by initial conditions. Note that $1 \pm a_i|V_i'| = 0$ is a fixed point of Eq. (5) and so the argument of the logarithm in Eq. (6) is always positive. The solution branch $|a_i||V_i'| < 1$ contains the RT late time asymptotics, and thus is the physical branch. Since dt' is a positive multiple of dt, we must choose $t' > t_0'$, and then the branch $a_i > 0$ is selected. With this choice, $0 < f_{i0} < 1$.

Solving Eq. (6) for $|V_i'|$ gives the scaled velocities

$$|V_i'| = \frac{e^{2a_i(t'-t_0')} - f_{i0}}{a_i(e^{2a_i(t'-t_0')} + f_{i0})}. \tag{7}$$

Noticing that

$$|V_i'| \equiv \frac{1}{\sqrt{Ag|Z_i|}} \frac{d|Z_i|}{dt} = \frac{d\ln|Z_i|}{dt'}, \tag{8}$$

and substituting Eq. (8) into Eq. (7), we have

$$\frac{d\ln|Z_i|}{dt'} = \frac{e^{2a_i(t'-t_0')} - f_{i0}}{a_i(e^{2a_i(t'-t_0')} + f_{i0})}. \tag{9}$$

Integrating Eq. (9) and using the formula

$$\int \frac{dx}{a+be^{mx}} = \frac{1}{am}[mx - \ln(a+be^{mx})], \tag{10}$$

we find that the trajectories of the RT mixing fronts are given by

$$|Z_i| = |Z_{i0}| \left[\frac{f_{i0} + e^{2a_i(t'-t_0')}}{1+f_{i0}} \right]^{1/a_i'} e^{-(t'-t_0')/a_i}, \tag{11}$$

where $Z_{i0} \equiv Z_i(t_0')$. Substituting Eq. (11) into Eq. (7), the (unscaled) velocity of the RT mixing front can be expressed as

$$|V_i| = \sqrt{Ag|Z_{i0}|} \frac{(e^{2a_i(t'-t_0')} - f_{i0})}{a_i(e^{2a_i(t'-t_0')} + f_{i0})} \left[\frac{f_{i0} + e^{2a_i(t'-t_0')}}{1+f_{i0}} \right]^{1/2a_i^2} \times e^{-(t'-t_0')/2a_i}. \tag{12}$$

Next we determine the relationship between t and t'. Substituting Eq. (11) into $dt' = dt\sqrt{Ag/|Z_i|}$ gives

$$\sqrt{Ag}\, dt = dt' |Z_{i0}|^{1/2} \left[\frac{f_{i0} + e^{2a_i(t'-t_0')}}{1+f_{i0}} \right]^{1/2a_i^2} e^{-(t'-t_0')/2a_i}, \tag{13}$$

and therefore the relationship between t and t' is given by

$$t - t_0 = \sqrt{\frac{|Z_{i0}|}{Ag}} \int_{t_0'}^{t'} \left[\frac{f_{i0} + e^{2a_i(t'-t_0')}}{1+f_{i0}} \right]^{1/2a_i^2} e^{-(t'-t_0')/2a_i} dt'. \tag{14}$$

Clearly, for any value of a_i, this integral can be evaluated numerically. It determines $t = t(t')$ as a function of t'. Substituting the functional inverse of Eq. (14), $t' = t'(t)$, into Eqs. (11) and (12) determines the entire dynamical evolution of the RT mixing fronts.

To illustrate the information contained in this solution, we consider its late time asymptotics. At late time, $t' \gg t_0'$. We rewrite Eq. (14) as

$$(1+f_{i0})^{1/2a_i^2} \sqrt{\frac{Ag}{|Z_{i0}|}} (t - t_0) = \int_{t_0'}^{t'} [1 + f_{i0} e^{-2a_i(t'-t_0')}]^{1/2a_i^2} \times e^{(t'-t_0')/2a_i} dt' \equiv I_1. \tag{15}$$

Integrating Eq. (15) by parts, we obtain

$$I_1 = 2a_i \left\{ [1 + f_{i0} e^{-2a_i(t'-t_0')}]^{1/2a_i^2} e^{(t'-t_0')/2a_i} - (1+f_{i0})^{1/2a_i^2} + \frac{f_{i0}}{a_i} I_2 \right\}, \tag{16}$$

where

$$I_2 \equiv \int_{t_0'}^{t'} [1 + f_{i0} e^{-2a_i(t'-t_0')}]^{(1-2a_i^2)/2a_i^2} \times e^{(t'-t_0')[(1-4a_i^2)/2a_i]} dt'. \tag{17}$$

Similarly, integrating I_2 by parts gives

$$I_2 = \left(\frac{2a_i}{1-4a_i^2} \right) \{ [1 + f_{i0} e^{-2a_i(t'-t_0')}]^{(1-2a_i^2)/2a_i^2} \times e^{(t'-t_0')[(1-4a_i^2)/2a_i]} - (1+f_{i0})^{(1-2a_i^2)/2a_i^2} \} + I_3, \tag{18}$$

where

$$I_3 \equiv \frac{2\, f_{i0}(1-2a_i^2)}{1-4a_i^2} \int_{t_0'}^{t'} [1 + f_{i0} e^{-2a_i(t'-t_0')}]^{(1-4a_i^2)/2a_i} \times e^{(1-8a_i^2)/2a_i^2} dt'. \tag{19}$$

Here we see that since $a_i^2 \geqslant 1/2$, I_3 is small relative to I_1 and I_2, i.e., $I_3 \ll I_2 \ll I_1$, for $t' \gg t_0'$. Thus, neglecting the smaller terms $\leqslant O(I_3)$, and substituting I_2 into I_1, we have the approximate evaluation

$$I_1 = 2a_i \left\{ [1 + f_{i0} e^{-2a_i(t'-t_0')}]^{1/2a_i^2} e^{(t'-t_0')/2a_i} - (1+f_{i0})^{1/2a_i^2} + \left(\frac{2\, f_{i0}}{1-4a_i^2} \right) \times \{ [1 + f_{i0} e^{-2a_i(t'-t_0')}]^{(1-2a_i^2)/2a_i^2} e^{(t'-t_0')[(1-4a_i^2)/2a_i]} - (1+f_{i0})^{(1-2a_i^2)/2a_i^2} \} \right\}. \tag{20}$$

For large t', $e^{-(t'-t_0')} \ll 1$. Using the Taylor series expansion and letting $x \equiv e^{(t'-t_0')/2a_i}$, we further write Eq. (20) in the form

$$I_1 = 2a_i x \left(1 - \frac{\gamma_1}{x} + \frac{\gamma_2}{x^{4a_i^2}} + \frac{\gamma_3}{x^{8a_i^2}} \right), \tag{21}$$

where

$$\gamma_1 \equiv (1+f_{i0})^{1/2a_i^2} \left(1 + \frac{2\, f_{i0}}{(1+f_{i0})(1-4a_i^2)} \right), \tag{22}$$

$$\gamma_2 \equiv \frac{f_{i0}}{2a_i^2(1-4a_i^2)} \quad \text{and} \quad \gamma_3 \equiv \frac{f_{i0}^2(1-2a_i^2)}{a_i^2(1-4a_i^2)}. \tag{23}$$

At late time, $x \gg 1$, $x^{-2} \ll x^{-1}$. Noticing that $a_i^2 \geqslant 1/2$ and ignoring high order terms, we obtain

$$(1+f_{i0})^{1/2a_i^2}\sqrt{\frac{Ag}{|Z_{i0}|}}(t-t_0) \approx 2a_i x\left(1-\frac{\gamma_1}{x}\right). \tag{24}$$

Therefore the relationship between $t'-t_0'$ and $t-t_0$ is

$$e^{(t'-t_0')/2a_i} \equiv x = \gamma_1 + \frac{(1+f_{i0})^{1/2a_i^2}}{2a_i}\sqrt{\frac{Ag}{|Z_{i0}|}}(t-t_0). \tag{25}$$

In terms of x, the trajectory and velocity of the mixing fronts in Eqs. (11) and (12) become

$$|Z_i(t)| = \frac{|Z_{i0}|}{(1+f_{i0})^{1/a_i^2}}(1+f_{i0}x^{-4a_i^2})^{1/a_i^2}x^2 \tag{26}$$

and

$$|V_i| = \frac{\sqrt{Ag|Z_{i0}|}}{a_i(1+f_{i0})^{1/2a_i^2}}\left(1-\frac{f_{i0}}{x^{4a_i^2}}\right)\left(1+\frac{f_{i0}}{x^{4a_i^2}}\right)^{(1-2a_i^2)/2a_i^2} x. \tag{27}$$

For large t', $x \gg 1$ so these solutions have the approximations

$$|Z_i(t)| = \frac{|Z_{i0}|}{(1+f_{i0})^{1/a_i^2}}\left(1+\frac{f_{i0}}{a_i^2}x^{-4a_i^2}\right)x^2 \tag{28}$$

and

$$|V_i| = \frac{\sqrt{Ag|Z_{i0}|}}{a_i(1+f_{i0})^{1/2a_i^2}}\left[1-\frac{(4a_i^2-1)f_{i0}}{2a_i^2x^{-4a_i^2}}+\frac{f_{i0}^2(1-2a_i^2)}{2a_i^2x^{-8a_i^2}}\right]x. \tag{29}$$

We now examine the late time trajectories of the mixing fronts. Substituting the expression (25) into Eq. (28), for $a_i^2 > 1/2$ (in most cases), the second term in Eq. (28) is negligible compared with the first term. We then get

$$|Z_i(t)| \approx \frac{1}{4a_i^2}Ag(t-t_0)^2 + \frac{\gamma_1}{a_i}(1+f_{i0})^{-1/2a_i^2} \times \sqrt{Ag|Z_{i0}|}(t-t_0) + \frac{\gamma_1^2|Z_{i0}|}{(1+f_{i0})^{1/a_i^2}}. \tag{30}$$

Substituting Eq. (25) into Eq. (29) and neglecting the high order terms $O(x^{-4a_i^2})$ for large t, we obtain the late time velocities of the mixing fronts,

$$|V_i| \approx \frac{\sqrt{Ag|Z_{i0}|}}{a_i(1+f_{i0})^{1/2a_i^2}}x = \frac{1}{2a_i^2}Ag(t-t_0) + \frac{\gamma_1\sqrt{Ag|Z_{i0}|}}{a_i(1+f_{i0})^{1/2a_i^2}}. \tag{31}$$

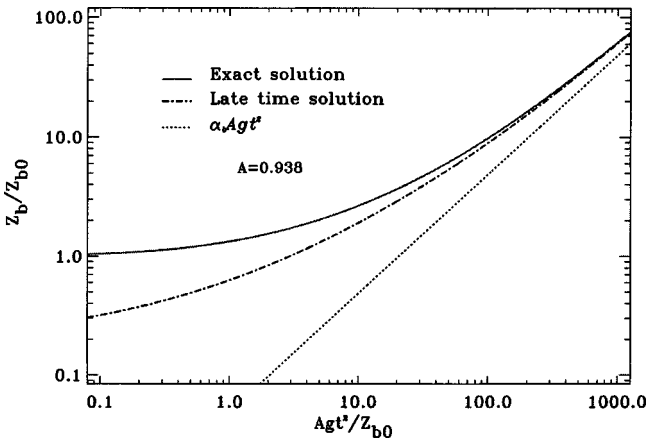

FIG. 1. The entire dynamical evolution of the trajectory of the bubble front for $A=0.938$. The solid line represents the exact solution, the dashed line denotes the late time asymptotic solution, and the dotted line gives the pure leading order asymptotic solution.

We see from Eqs. (30) and (31) that the corrections to the leading order expressions for $|Z_i|$ and $|V_i|$ depend on the initial conditions. This result is consistent with recent numerical simulations of Youngs [16].

The entire dynamical evolution of the trajectory of the mixing fronts (for both early and late time) is computed numerically. The results are shown in Fig. 1, where we have plotted the exact solution for the bubble front at Atwood number $A=0.938$ as a solid line. The dashed line represents the late time asymptotic solution and the dotted line denotes the full leading order approximations to the late time asymptotics. From Fig. 1, we see that the full asymptotic solution approaches the exact solution and represents it well even for rather modest values of Z_b/Z_{b0}, while the pure leading order asymptotics converges much more slowly. Of the three parameters Z_{i0}, V_{i0}, and t_0 needed to set the initial conditions for Eq. (5), only two specify independent solutions, as the third amounts to translation along a solution trajectory. In this log-log plot, the slope is determined by the exponent 2 in t^2, and the intercept is determined by the growth constant α_b. Thus both are determined by the leading order asymptotics. The deviation from linearity is determined by the lower than leading order terms. In more customary plots (linear in the Z and Agt^2 variables), the slope is determined by α_b, i.e., the leading order asymptotics, and the lower than leading order asymptotics determines the intercept of the growth curve with the coordinate axes, as well as any possible deviation from linearity. The nonzero intercepts are clearly visible in some of the experimental data and the deviation from linear growth in Agt^2 is clearly visible in most simulation studies, as we see below.

To compare our exact solution with experimental data, we take experiments No. 103 ($A=0.938$) and No. 101 ($A=0.829$) conducted by Smeeton and Youngs [15] at the Atomic Weapons Establishment (AWE) as examples. The bubble drag coefficients for these two experiments, inferred from Eq. (3) and the experimentally determined value for α_b, is $C_b \sim 3.8$. Substituting these numbers into the equation, we obtain the solution for the bubble fronts corresponding to experiment 103 displayed in Fig. 2. Here

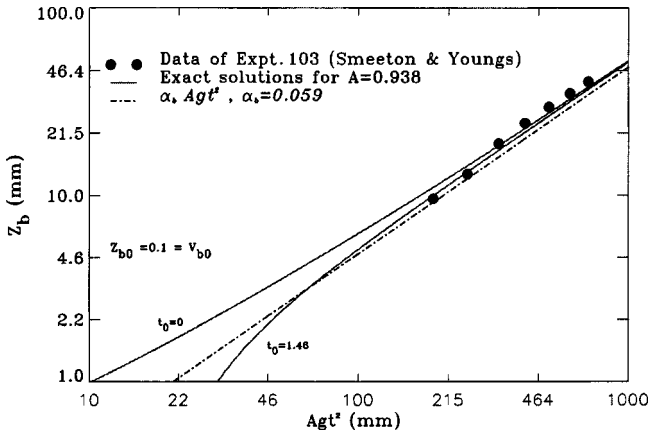

FIG. 2. Comparison of the exact solution, late time pure leading order asymptotic solution, and the experimental data. Multiple exact solutions are obtained by varying t_0 while Z_{b0} and V_{b0} are held fixed.

we have chosen $Z_{i0}=0.1=V_{i0}$ and used t_0 as a fitting parameter to obtain agreement with the experimental data. Thus the experimental slope and linear offset yields α_b, while the nonlinear offset or intercept gives t_0. This figure shows very good agreement between one of the calculated solutions and experiment 103, and provides a modest improvement to the pure leading order fit (the dot-dashed line in Fig. 2) to the data.

In Fig. 3, we show the solution dependence on Z_{i0}. As is clear from Fig. 3 or from Eq. (30), a positive Z_{i0} amounts to a shift of the solution upwards, and thus gives an intercept on the positive Z_i axis. From Fig. 2, we see that the influence of t_0 on the solution is primarily to shift the entire solution to the left or right. However, only the value $t_0>0$ should be admitted, corresponding to a shift of the solution to the right. Such a shift will give a solution which has an intercept on the Agt^2 axis, or at most a bounded distance along the Z_b axis, as occurs in Fig. 2. Similarly, only positive Z_{i0} should be admitted as initial data. It follows that a suitable choice of initial conditions will allow for an arbitrary positive intercept on either axis for the solution, by varying Z_{i0} or t_0, for example. However, the intercept does not uniquely determine

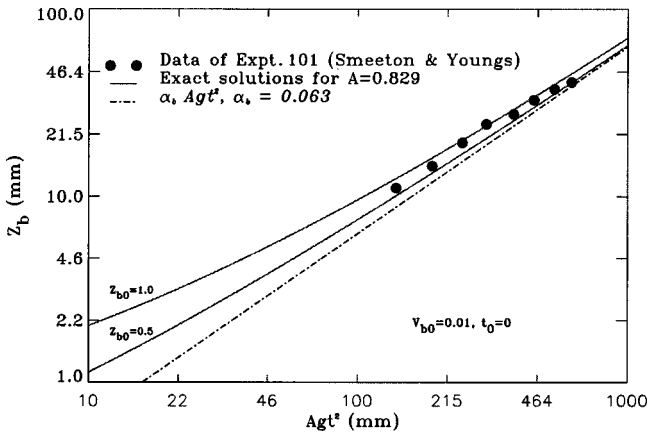

FIG. 3. Dependence of the exact solution on variation of initial data (Z_{i0}), while V_{b0} and t_0 are held fixed.

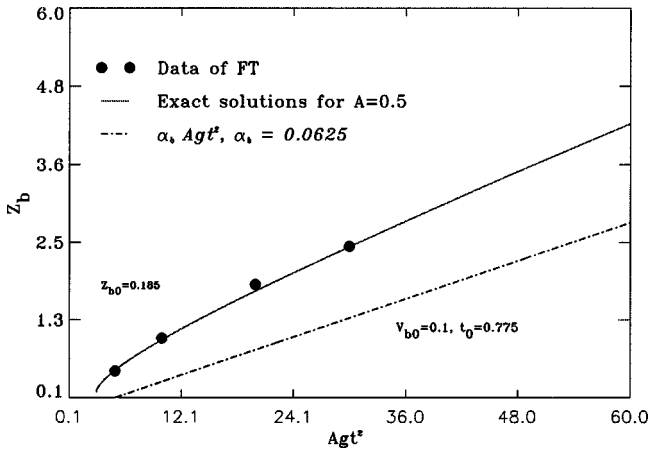

FIG. 4. Comparison of simulation data with the exact solution of the model equation. The model equation (solid curve) provides a possible explanation for the curvature of the data. The leading order asymptotics is shown as the dash-dotted straight line.

the ODE initial conditions. Our solution offers a theoretical explanation of these nonlinear log-log intercepts (i.e., the intercepts in the Z vs Agt^2 plots). The intercepts for the linearly plotted Z vs Agt^2 line are experimentally observable. The initial curvature, or deviation from linearity in the Z_i vs Agt^2 plane, occurs too early to be observed experimentally. We see in Fig. 3 that one of the solutions obtained by varying Z_{i0} agrees with the data from experiment 101. Our preferred solution, approximately $Z_{b0}=0.75$, bracketed by the two solid curves in Fig. 3, clearly fits the data of experiment 101 better than does the pure late time asymptotics (the dot-dashed curve in this figure).

In simulations data can be recorded at all times. The linearly plotted Z vs Agt^2 curvature or lower than leading order asymptotics of the solution may contribute to the observed dependence of α_b on time in the simulations. Simulations have not been carried to as late a dimensionless time as in the experiments, so the lower than leading order asymptotics could make a contribution in the analysis of simulation data. In Fig. 4, we take the front tracking (FT) simulations of Ref. [17], with Z_b plotted vs Agt^2 and compare with the solution of the buoyancy drag equation (1) with initial conditions $t_0=0.775$, $Z_{b0}=0.185$, and $V_{b0}=0.1$ for $A=0.5$ and $C_b=4.6$ which corresponds to an $\alpha_b\sim 0.0625$.

These parameters are determined as follows. Only two of the three initialization parameters t_0, Z_0, V_0 change the solution trajectory independently. Thus two parameters are used to make the solution pass through the first point of Fig. 4. The single remaining solution parameter, C_b, is modified to force the solution to fit the remaining three points. Thus C_b and $\alpha_b=\alpha_b(C_b)$ are determined directly from the simulation data. This method of determining α_b emphasizes the later time data, and for this reason, we obtain a lower value $\alpha_b=0.0625$ than the value $\alpha_b=0.07$ obtained previously, using a straight line fit to the data [17].

In order to see the whole picture we also replot these data in a logarithm scale in Fig. 5 and display the experimental data from experiment 101. In both figures, the dash-dotted line is the leading order asymptotics for this same value of

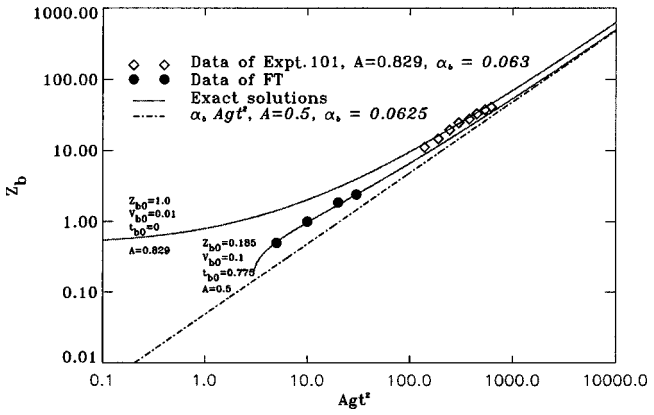

FIG. 5. Comparison of simulation data with the exact solution of the model equation in a large scale. The solid curves provide a possible explanation for the curvature of the preasymptotic simulation data and for the straight line of the asymptotic experimental data. The pure leading order asymptotics is shown in the dash-dotted straight line.

α_b. The data, for both simulation and experiment cover about one half decade of variation for Z_b or Agt^2. The experimental data relate these variables in a nearly linear manner, and a fit to the slope determines α_b. The simulation data are not close to linear, and so although the reported α_b was determined previously by a straight line fit, and it is here determined by a one parameter fit to nonlinear data, neither has the same significance as the linear fit to a nearly straight line, as with the experimental data. In any case, we believe that the value $\alpha_b=0.0625$ determined here on the basis of solutions to Eq. (1) improves on that determined earlier using a straight line fit. In both the experimental and simulation case, Eq. (1) offers preasymptotic behavior as a possible cause of the deviation from linearity of the data. Finally, we note that the simulation and experimental data cannot be compared directly. The axes in all the figures have units of length. For the experiments the length unit is determined in physical units, while the length unit for the simulation is arbitrary. However, to fit the simulation data and the experimental data in a single solution of Eq. (1) shows qualitatively the asymptotic regime of the experiment data and the preasymptotic regime of the simulation data.

In RM mixing, $g(t)=\delta(t)$. For $t>0$, Eq. (2) becomes

$$\frac{dV_i}{dt}=-(-1)^i C_i\,\frac{1-(-1)^i A}{2}\,\frac{V_i^2}{|Z_i|},\quad i=1,2. \tag{32}$$

In terms of the scaled variables, $V_i'\equiv V_i/\sqrt{A|Z_i|}$, $dt'\equiv dt\sqrt{A/|Z_i|}$, it reduces to

$$\frac{d|V_i'|}{dt'}=-\tfrac{1}{2}\{1+C_i[1-(-1)^i A]\}|V_i'^2|=-a_i^2|V_i'^2|. \tag{33}$$

This equation is easily solved by integrating twice with the results

$$|V_i'|=\left[\frac{1}{|V_{i0}'|}+a_i^2(t'-t_0')\right]^{-1},$$

$$|Z_i|=|Z_{i0}|[1+a_i^2|V_{i0}'|(t'-t_0')]^{1/a_i^2}. \tag{34}$$

The correlation function between $t-t_0$ and $t'-t_0'$ is found as

$$1+a_i^2|V_{i0}'|(t'-t_0')=\left[1+\sqrt{\frac{A}{|Z_{i0}|}}\,\frac{(1+2a_i^2)}{2}|V_{i0}'|(t-t_0)\right]^{2a_i^2/(1+2a_i^2)}. \tag{35}$$

Substituting this into Eq. (34), the trajectory and velocity of the RM mixing edges at time t are obtained as follows:

$$|Z_i(t)|=|Z_{i0}|\left[1+\frac{(1+2a_i^2)}{2|Z_{i0}|}|V_{i0}|(t-t_0)\right]^{2/(1+2a_i^2)} \tag{36}$$

and

$$|V_i(t)|=|V_{i0}|\left[1+\frac{(1+2a_i^2)}{2|Z_{i0}|}|V_{i0}|(t-t_0)\right]^{(1-2a_i^2)/(1+2a_i^2)}. \tag{37}$$

These solutions are consistent with the solutions in Ref. [18], with the added feature that the exponents and coefficients in Eqs. (36) and (37) are here explicitly related to the drag coefficient and Atwood number.

For large t, the trajectory and the velocity of the mixing front of phase i have the asymptotic behavior

$$|Z_i(t)|\sim|Z_{i0}|^{(1-\theta_i)}|V_{i0}|^{\theta_i}\theta_i^{-\theta_i}(t-t_0)^{\theta_i} \tag{38}$$

and

$$|V_i(t)|\sim|Z_{i0}|^{(1-\theta_i)}|V_{i0}|^{\theta_i}\theta_i^{1-\theta_i}(t-t_0)^{\theta_i-1}, \tag{39}$$

where $\theta_i\equiv 2/(1+2a_i^2)$. Clearly, for $A=1$, $\theta_s=1$. This result agrees with theory and with existing experiment data. We also see that unlike RT mixing, the dynamical evolution of the mixing layer in RM mixing always depends strongly on the initial conditions.

IV. CONCLUSIONS

A complete, closed form solution for the edges of the mixing zone of acceleration driven RT and RM mixing layers is given; in the RT case, the solution contains a quadrature. The late time RT asymptotics, through terms which are $O(1)$ in t, is obtained approximately in closed form.

The solution is based on a buoyancy-drag ODE, with a previously validated choice of drag coefficient. The solutions provide the clearest explanation offered to date of the often

noted fact that RT mixing loses memory of its initial conditions, while RM mixing does not. RT mixing, even for steady acceleration, satisfies a uniform growth law proportional to t^2 only to leading order in the late time asymptotics, while the lower order growth terms break this law and also display dependence on initial conditions. Our analysis shows this RT dependence on initial conditions. The RT dependence on initial conditions can be seen in the experimental data and even more clearly in the simulation data.

ACKNOWLEDGMENTS

B.C. and J.G. were supported by the U.S. Department of Energy, under Contract No. W-7405-ENG-36. D.H.S. was supported by the U.S. Department of Energy Contract Nos. DE-FG02-90ER25084, DE-AC02-98CH10886, the Department of Energy Office of Inertial Fusion, the Army Research Office, Grant No. DAAD-19-01-1-0642, and the National Science Foundation, Grant No. DMS-0102480.

[1] S. Chandrasekhar, *Hydrodynamic and Hydromagnetic Stability* (Oxford University Press, Oxford, 1961).
[2] D. H. Sharp, Physica D **12**, 3 (1984).
[3] J. Glimm and D. H. Sharp, in *Stochastic Partial Differential Equations: Six Perspectives*, edited by R. A. Carmona and B. L. Rozovskii, Mathematical Surveys and Monographs (American Mathematical Society, Providence, 1997).
[4] *Proceedings of the 4th International Workshop on the Physics of Compressible Turbulent Mixing*, edited by P. F. Linden, D. L. Youngs, and S. B. Dalziel (Cambridge University Press, Cambridge, England, 1993).
[5] *Proceedings of the Fifth International Workshop on Compressible Turbulent Mixing*, edited by R. Young, J. Glimm, and B. Boston (World Scientific, Singapore, 1996).
[6] B. Cheng, J. Glimm, and D. H. Sharp, Phys. Lett. A **268**, 366 (2000).
[7] D. L. Youngs, Physica D **37**, 270 (1989).
[8] U. Alon, J. Hecht, D. Mukamel, and D. Shvarts, Phys. Rev. Lett. **72**, 2867 (1994).
[9] U. Alon, J. Hecht, D. Ofer, and D. Shvarts, Phys. Rev. Lett. **74**, 534 (1995).
[10] G. Dimonte and M. Schneider, Phys. Rev. E **54**, 3740 (1996).
[11] G. Dimonte, Phys. Plasmas **6**, 2009 (1999).
[12] G. Dimonte and M. Schneider, Phys. Fluids **12**, 304 (2000).
[13] L. Landau and E. Lifshitz, *Fluid Mechanics* (Addison-Wesley, Reading, MA, 1959).
[14] D. Oron, L. Arazi, D. Kartoon, A. Rikanati, U. Alon, and D. Shvarts, Phys. Plasmas **8**, 2883 (2001).
[15] V. S. Smeeton and D. L. Youngs, AWE Report Number O 35/87, 1987 (unpublished).
[16] D. L. Youngs (private communications).
[17] E. George, J. Glimm, X. L. Li, A. Marchese, and Z. L. Xu, Proc. Natl. Acad. Sci. U.S.A. **99**, 2587 (2002).
[18] J. D. Ramshaw, Phys. Rev. E **58**, 5834 (1998).